Journal of Materials Chemistry A

ROYAL SOCIETY OF CHEMISTRY

PAPER

View Article Online
View Journal | View Issue

Cite this: *J. Mater. Chem. A*, 2021, **9**, 6913

Functional sponge-based triboelectric nanogenerators with energy harvesting, oil–water separating and multi-mode sensing performance†

Shuai Liu,[a] Fang Yuan,[a] Min Sang,[b] Jianyu Zhou,[a] Junshuo Zhang,[a] Sheng Wang,*[a] Jinsong Li,[c] Shouhu Xuan [ad] and Xinglong Gong *[a]

Lack of fossil oil and pollutant leakage pose global challenges to human society. Developing smart energy-generation devices with controllable oil adsorption performance might be a significant attempt to cope with the crisis. Here, an advanced triboelectric nanogenerator (TENG) with mechanical/magnetic energy harvesting and smart oil–water separating performance was fabricated by assembling a magnetic sponge with a conductive polymer film. The sponge was facilely prepared by dispersing carbonyl iron into Ecoflex using a sugar sacrificial templating technique. The TENG presents favorable triboelectric performance with an optimal power density of 71.0 mW m^{-2} at 5 MΩ. Thus, it can power small electronics and serve as a wearable sensor to monitor various human gaits. Besides, the sponge-based TENG generates a notable signal of 495 mV in response to 540 mT, indicating the capability of self-powered sensing external magnetic fields *via* gathering the magneto-actuated deformation energy. More importantly, the hydrophobicity and lipophilicity effects endow the TENG with oil–water separation property, and it exhibits a desirable magneto-driving and target recognition capacity. Finally, the TENG-based sensor array with sensitive mechanical–magnetic dual-mode response can accurately map external stimuli distributions, and the integrated wireless system reveals the feasibility in miniaturized portable electronics. Thus, this work provides an instructive strategy for the development of versatile TENG devices in multiple energy collection and oil–water separation.

Received 21st December 2020
Accepted 3rd February 2021

DOI: 10.1039/d0ta12359e

rsc.li/materials-a

1. Introduction

The rapid flourish in smart electronics in recent years has motivated the development of clean and sustainable power sources.[1–3] Owing to the limited availability of fossil fuel, harvesting ubiquitous mechanical energy from the environment provides an effective approach to balance the energy crisis.[4,5] Triboelectric nanogenerators (TENGs), based on the coupling effects of triboelectrification and electrostatic induction, are able to harvest mechanical energy from deformations,[6] human motions,[7] airflows[8] and ocean currents[9] *via* charge migration. Besides, TENGs have attracted considerable attention as reliable self-powered sensing systems in detecting various external stimuli.[10,11] Recently, developing multifunctional TENG devices has become a hot research topic due to the complicacy of application conditions. For instance, by growing conductive polyaniline nanowires onto a polymer substrate, an innovative TENG successfully implemented toxic NH_3 sensing property in addition to harvesting mechanical energy.[12] By designing a distinct translational rotary magnetic structure, a multifunctional TENG-based sensor could detect acceleration and force, as well as the rotational parameters.[13] Moreover, an anti-impact polymer composite endowed a versatile TENG with favorable impact energy collecting and safeguarding performance, which widen its practical applications.[14] Thus, it is an effective strategy to endow TENGs with novel properties by integrating functional nano-fillers or designing new structures.

Developing integrated TENGs with universal stimuli-sensing and various energy-harvesting performance is one of the mainstream trends, which aims to improve adaptability to complex circumstances.[15,16] Typically, magnetic field is widespread and the important applications in industrial and practical life motivate the exploration of magnetic detection technology.[17,18] The magneto-induced deformation offers an effective strategy in response to magnetic field, and meanwhile, it is an important energy source. Owing to the large specific surface area, low elastic modulus and light weight, magnetic

[a]CAS Key Laboratory of Mechanical Behavior and Design of Materials, Department of Modern Mechanics, CAS Center for Excellence in Complex System Mechanics, University of Science and Technology of China (USTC), Hefei 230027, P. R. China. E-mail: wsh160@ustc.edu.cn; gongxl@ustc.edu.cn

[b]Department of Chemistry, University of Science and Technology of China, Hefei, Anhui 230026, PR China

[c]MSC (Beijing) Technical Service Co., Ltd, Beijing, 100102, PR China

[d]National Synchrotron Radiation Laboratory, University of Science and Technology of China, Hefei, 230027, PR China

† Electronic supplementary information (ESI) available. See DOI: 10.1039/d0ta12359e

three-dimensional porous sponges could generate remarkable deformations under the actuation of magnetic field.[19,20] Thus, sponge-based TENGs, apart from the inherent mechanical energy harvesting performance, might be a significant attempt for monitoring and collecting magnetic energy. However, few works have concentrated on porous-structured multi-mode functional TENGs and the based self-powered sensors up to now.

However, developing environment-friendly TENGs becomes another important issue in consideration of the increasingly serious environmental pollution.[21] For example, airborne particulate matter exerted detrimental effects on human health, and a TENG-based negative air ion generator was developed to effectively ionize the air molecules for indoor air purification.[22] Since oil/organic solvent leakage caused dramatic damage to ecological and economic systems, porous sponge composites are considered as ideal absorbent materials due to the high selective absorption and convenient transport properties.[23,24] Thus far, various sponges based on polydimethylsiloxane (PDMS),[23] polyurethane[25] and melamine[26] have been proposed for efficient oil–water separation, which propelled the progress of spill cleanup and fuel purification. However, previous works have mainly focused on the oil–water separation capability, and little attention is paid to the intelligent sensing and magnetic driving/removing performance for contaminants from aquatic environments. Thus, magnetic sponge-based TENGs, owing to the inherent self-powered sensing effect, might be beneficial for distinguishing pollutants of oily wastewater. More importantly, the magneto-responsive capacity provides magnetic sponges with the possibility for precise control in intelligent oil–water separation systems. Regrettably, such a smart all-in-one TENG device has not been developed yet.

Thus, in this work, a sponge-based environment-friendly multifunctional TENG with force/magnetic-dependent triboelectric properties and oil–water sensing/removing performance was designed by assembling a magnetic CI–Ecoflex sponge with a conductive MWCNT/CI–PDMS composite. The sponge was fabricated by embedding CI particles into an Ecoflex matrix using a sugar sacrificial templating technique. The newly designed TENG shows effective mechanical energy harvesting performance with a high instantaneous power density of 71.0 mW m^{-2} at 5 MΩ. Therefore, it can not only power stopwatch electronics, but also serve as a wearable device to monitor human motions. The sponge displays remarkable magneto-actuating deformation with a typical deformation rate of 30% under 540 mT, and hence the based TENG can monitor the magnetic field attributed to the deformation-induced triboelectric effect. More importantly, owing to the intrinsic hydrophobicity and oleophilicity of the sponge, the based TENG, as a smart absorbent material, shows potential in oil–water separation and sensing various contaminants. Finally, the TENG-based sensor array serves well in mechanical–magnetic bi-mode sensing fields, which can precisely recognize their distributions, and the integration with wireless transmission module can greatly contribute to the large-scale applications. Therefore, this novel TENG device demonstrates to be a promising candidate for multi-functional portable electronics, self-powered magnetic detection and controllable oil spill recovery.

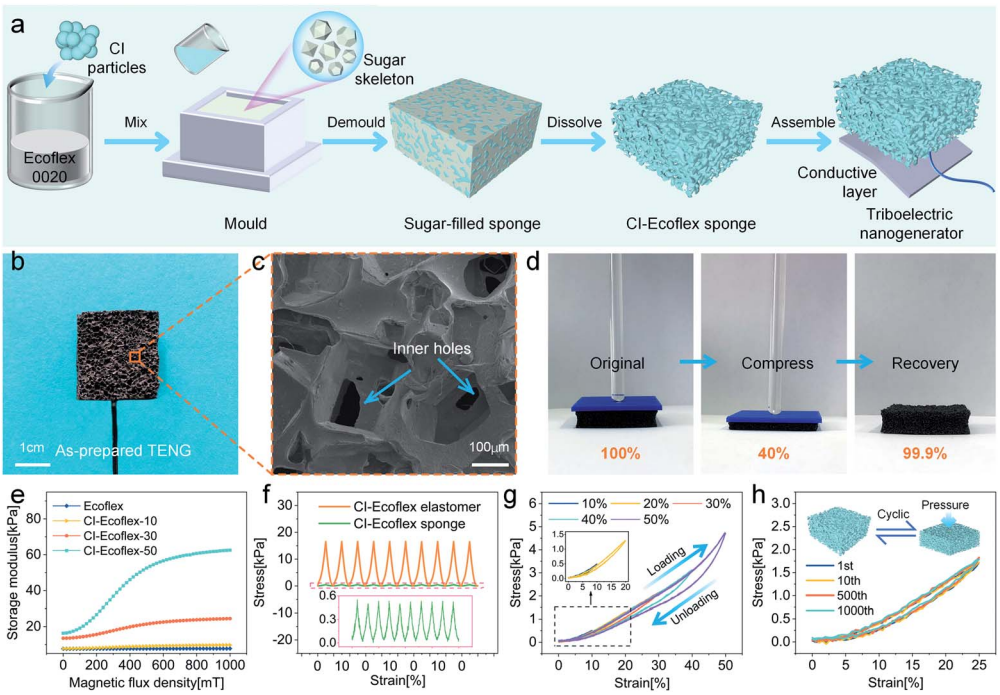

Fig. 1 Preparation and characterization of the composites. (a) Schematic of the fabrication and (b) photograph of the TENG device. (c) SEM image of the porous sponge. (d) Compression-recovery property of the sponge. (e) Magnetorheological properties of the sponges with various CIs. (f) Strain-dependent stress of the sponge and elastomer. (g) Strain–stress curves of the sponge at various compressive strains. (h) Robustness of the sponge under 1000 cycles at 25% compressive strain.

2. Results and discussion

2.1. Material design and property characterization

The fabrication procedures of TENG are illustrated in Fig. 1a. Briefly, The Ecoflex pre-polymer with CI particles was cast into the as-prepared mould. The sacrificial template of the interconnected water-soluble sugar skeleton in the mould was aimed to produce a porous structure in the CI–Ecoflex elastomer. After curing, deionized (DI) water was utilized to remove the sugar. Finally, the dried sponge was assembled with a conductive MWCNT/CI–PDMS layer to acquire this novel TENG (Fig. 1b). The SEM image of the sponge (Fig. 1c) revealed that it consisted of an interconnected template geometry-dependent 3D porous structure. Originated from the low modulus and high porosity of the polymer matrix, the sponge exhibited favorable compressibility and recoverability properties (Fig. 1d).

In this work, a sponge matrix with different CI contents was prepared to optimize the multi-functional performance of the TENG. For convenience, the sponge with different CIs was defined as CI–Ecoflex-*X*, where *X* is the fraction of CIs. As shown in Fig. 1e, the storage modulus of CI–Ecoflex increased as the magnetic flux density raised, showing typical magneto-rheological properties. In particular, CI–Ecoflex-50 exhibited a remarkable magnetorheological effect of 284.6%, which was much larger than that of other composites. However, the increase in CI content would impede the fluidity of uncured CI–Ecoflex, which made it difficult to prepare sponge with more CIs (Fig. S1†). Hence, CI–Ecoflex-50 with the fastest response to magnetic field was favorable for further study. Besides, after a comprehensive consideration of the conductivity, viscosity and the effect on output performance (Fig. S2†), CI and MWCNT with a mass ratio of 50% and 2% with the PDMS polymer were selected as the suitable conductive layer.

Peak stress of the CI–Ecoflex sponge was 0.5 kPa and much lower than 16.5 kPa of the non-porous elastomer during the cyclic strain (10%) loading–unloading process (Fig. 1f), demonstrating a significant improvement in flexibility. Unloading stress branch of the sponge could return to the initial level (Fig. 1g), indicating its excellent elastic deformation behavior. In addition, the stress–strain curves remained stable after 1000 cycles of loading–unloading excitations (Fig. 1h), which guaranteed its reliable mechanical property in practical applications.

2.2. Mechanical energy harvesting performance of the TENG

Fig. 2a schematically illustrates the working mechanism of the TENG. As a typical passive device, the energy harvesting property was based on the contact electrification and electrostatic induction effect.[27,28] When a substance came in contact with the TENG, electrons would shift from the interface of the substance to the sponge matrix due to the difference in electronegativity (Fig. 2a-I). As the substance was separating away, the two surfaces with opposite charges generated a potential difference, which was corresponding to the trend of numerical simulation (Fig. S3†). The negative charges would induce positive ones on

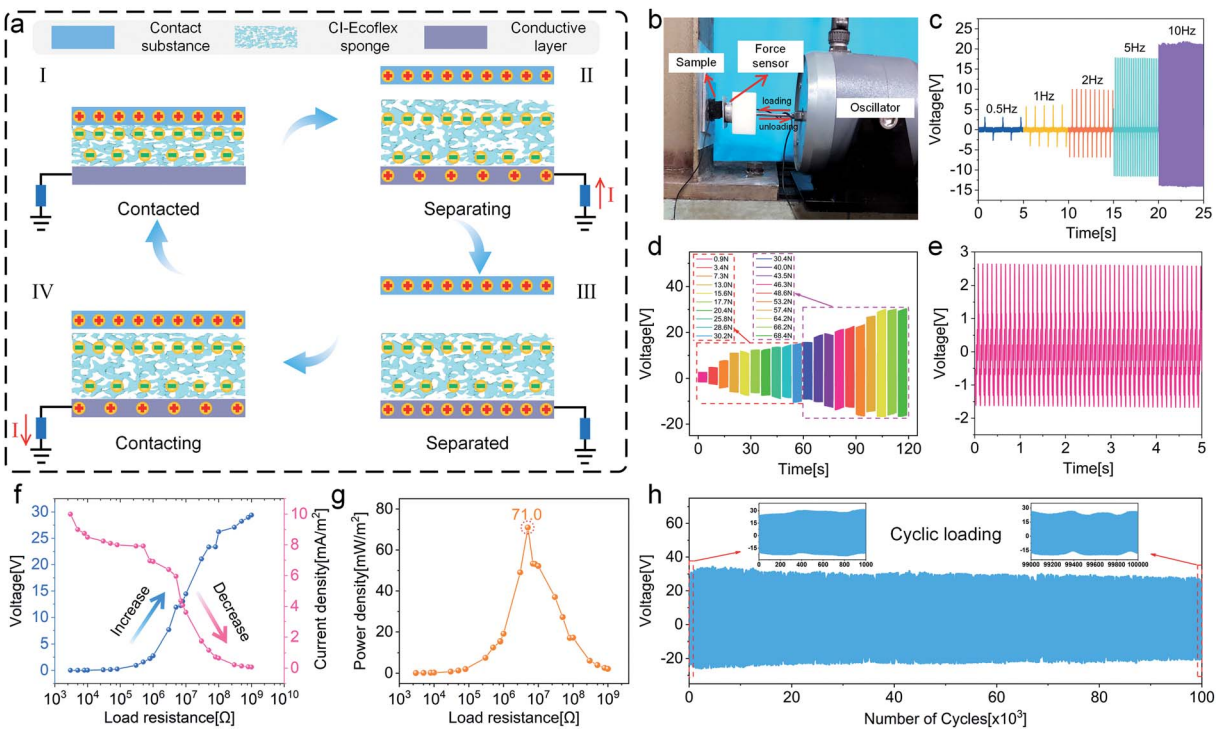

Fig. 2 Triboelectric performance of the TENG. (a) Schematic of the working mechanism. (b) The measurement system. (c) Real-time voltages of TENG subjected to different frequencies of 0.5–10 Hz. (d) Force-dependent output voltages at 10 Hz. (e) Typical voltage signals under 0.9 N. (f) Voltage, current density and (g) instantaneous power density under different external load resistances. (h) Voltage stability of TENG under cyclic excitations of 64.2 N and 10 Hz.

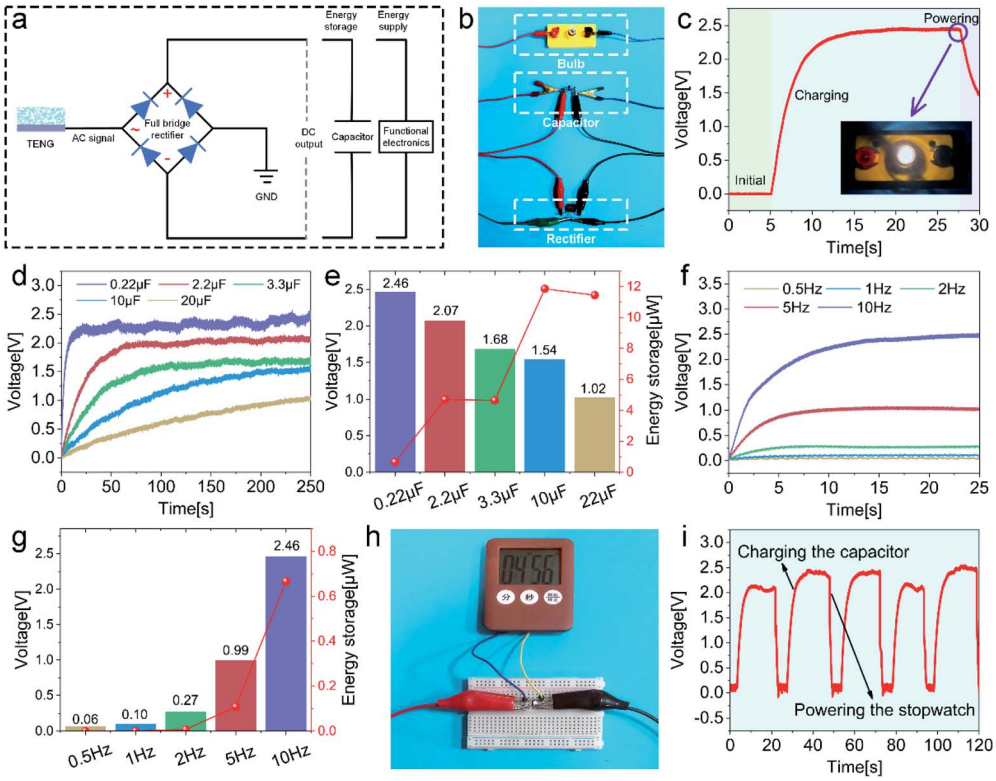

Fig. 3 Energy storage and application of the TENG. TENG-based (a) rectifier circuit diagram and (b) photograph of harvesting mechanical energy to power electronics. (c) Voltage variation for powering a bulb. (d) Capacitance-dependent charging behaviors at a frequency of 10 Hz. (e) Voltage (bar graph) and energy storage (line chart) in various capacitors after charging for 250 s. (f) Influence of the loading frequency on charging behaviors for a 0.22 μF capacitor. (g) Voltage (bar graph) and energy storage (line chart) in the capacitor after charging for 25 s. (h) TENG powering a stopwatch. (i) Cyclic charge–discharge curve.

the conductive layer, so as to reach an electrostatic equilibrium. Therefore, the free electrons were driven to flow from the electrode to the ground, thus generating current and voltage outputs (Fig. 2a-II). When the substance left far away, the system reached electrostatic equilibrium (Fig. 2a-III). As the substance approached again, the induced positive charges in the conductive layer were decreased, which would result in a reverse electron flow (from the ground to the electrode), contributing to an opposite directional voltage signal (Fig. 2a-IV) until it returned to the initial state. Subjected to varying external excitations, different deformations and contact areas were induced on the TENG, which led to the stimulus-dependent charge transfer and the corresponding output voltage signals.

The triboelectric performance measurement system is presented in Fig. 2b. The tested TENG with a dimension of $2 \times 2 \times 1$ cm^3 was fixed on a flat plate, and external excitations were loaded by an oscillator. First, the contact force and loading frequency-dependent triboelectric properties were studied. Keeping the force at 47 N, the voltage raised from 3.1 to 21.5 V as the loading frequency increased from 0.5 to 10 Hz, demonstrating a positive correlation between electric signal and applied frequency (Fig. 2c). As the loading frequency further increased, the voltage tended to be saturated at 10 Hz (Fig. S4†), which could suitably demonstrate the energy harvesting performance. Besides, in consideration of the relatively few high-frequency excitations in daily life, it was of greater guiding significance for practical applications to adopt 10 Hz for further investigation. Fig. 2d presents the real-time generated voltage signals corresponding to different contact forces (Fig. S5†) at 10 Hz. With the progressive increment of applied force, the output voltage increased and ultimately approached to saturation. For example, the voltage increased from 4.8 to 29.6 V as the contact force rose from 3.4 to 64.2 N, and it showed a tiny increment (from 29.6 to 29.8 V) when the force was 68.4 N. Besides, TENG showed high sensitivity to 0.9 N by 2.6 V, exemplifying the favorable capacity of harvesting weak mechanical energy (Fig. 2e). In summary, under the working condition of 64.2 N and 10 Hz, triboelectric performance of the TENG obtained optimal values.

Considered as a sustained power source, the influence of external load resistances on output properties of TENG was systematically explored. When the resistance increased, the output voltage showed an increasing trend rising from 0.01 to 29.4 V, while the current density exhibited an opposite declining tendency from 4.0 to 0.03 μA (Fig. 2f). Fig. 2g exhibits the maximum instantaneous power density of 71.0 mW m^{-2} at 5 MΩ. Besides, the stable voltage during cyclic loading–unloading stimuli for 10^5 cycles proved that the TENG possesses reliable mechanical as well as electrical properties (Fig. 2h).

Owing to the inherent pulse-type output performance of alternating current (AC) signals, the TENG could not directly drive electronic devices. Capacitors were generally utilized as energy storage units to store the triboelectric energy and further supply direct current (DC) power for electronic equipment. Fig. 3a and b shows the diagram of TENG to charge a 0.22 μF capacitor and power a bulb *via* a full bridge rectifier circuit. The corresponding voltage curve is presented in Fig. 3c. The charging voltage increased rapidly to 2.45 V within 20 s, and then the capacitor was connected with a bulb and lit it up (Movie S1†). In view of the energy storage properties, it was essential to investigate the charging behaviors for various capacitances (0.22–20 μF). The charging rate decreased with the increase in capacitance, in which the voltage of 0.22 μF capacitor was saturated within 20 s (Fig. 3d). The charging voltage (V_c) and energy storage (W_s, defined as $W_s = CV_c^2/2$) for various capacitors after charging for 250 s are summarized in Fig. 3e. Evidently, V_c showed a decreasing trend as the capacitance increased, and W_s attained the highest value of 11.86 μW at 10 μF capacitor, suggesting a more suitable energy storage unit. Besides, the dependence of charging performance on the loading frequency was studied. Higher loading frequencies contributed to the increase in V_c and W_s (Fig. 3f and g). Furthermore, the TENG device, serving as an effective power supplier, could charge a 0.22 μF capacitor to about 2.46 V and a commercial stopwatch could be successfully driven to operate (Fig. 3h and Movie S2†). These charge–discharge processes were cyclic stable, demonstrating the high reliability of this system (Fig. 3i). Thus, this TENG showed considerable potential as a new environment-friendly, cost-effective and sustainable power source.

Since the TENG device could generate voltage signals under mechanical stimuli, it could serve as a distinct force sensor to perceive various external excitations (Fig. 4a). For instance, it could actively sense external finger tapping pressures by outputting electric signals (Fig. 4b and c). As the number of operating fingers increased, the average peak voltage showed an enhancement from 2.6 to 3.2 V, which could be used to distinguish the contact areas. In addition, owing to the light weight and favorable flexibility, the TENG sensor could serve as a wearable device to monitor diverse human motions (Fig. S6†). For example, Fig. 4d–f and g–i presented the sensing signals on a commercial force sensor and the as-designed self-powered TENG sensor during walking, running and stamping process. This sensor showed fast dynamic response to the movements of stepping on and off, and the distinguished voltage amplitudes and frequencies could be used to recognize multiple gait patterns. More importantly, the voltage peak values of TENG were consistent with the force signals of the commercial sensor, indicating its good reliability and stability. Therefore, owing to

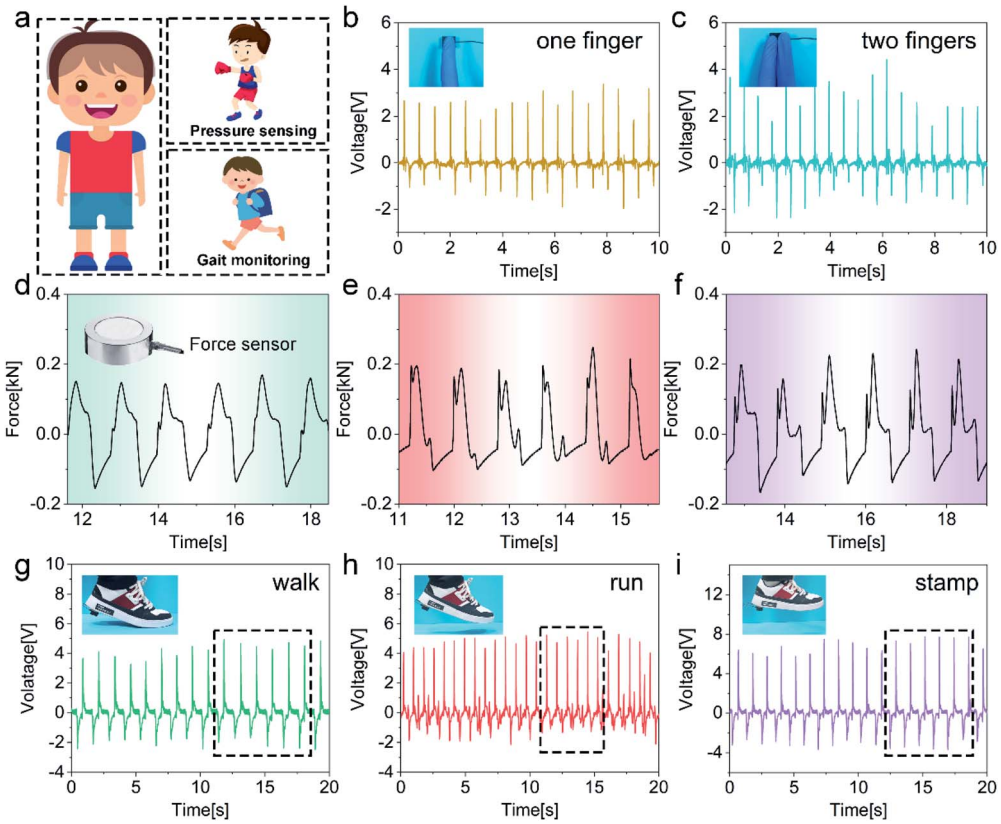

Fig. 4 Demonstration of the TENG as a self-powered force sensor for pressure and gait monitoring. (a) Schematic diagram of sensing application. The output voltages stimulated by continuous tapping with (b) one and (c) two fingers. Sensing signals of (d–f) a commercial force sensor and (g–i) this TENG sensor triggered by walking, running, and stamping, respectively.

the advantages of low cost, light weight and easy integration, this sensor showed excellent applicability for real-time motion recognition.

2.3. Self-powered magnetic field sensing property of the TENG

Generally, the magnetic field played a significant role in contact-less actuation, intelligent navigation and remote sensation fields, so it was of great importance to develop magnetic field sensing techniques. In this work, based on the synergic characteristics of magneto-actuated deformation and triboelectric effect, the as-fabricated TENG device could monitor external magnetic fields without additional power supply. Clearly, the magneto-actuated deformation derived from the introduction of CI particles. As shown in Fig. 5a, CI particles exhibited a remarkable soft magnetic property with a saturated magnetization intensity of 201.2 emu g^{-1}, while pure Ecoflex presented a negligible magnetization intensity value of 0.4 emu g^{-1}. Due to the intrinsic magnetization, the incorporation of CI endowed sponges with magnetic effect, in which the saturated magnetization intensities of CI–Ecoflex-30 and CI–Ecoflex-50 were 61.2 and 112.5 emu g^{-1}, respectively. Thus, the magnetic field-dependent triboelectric performance is further explored in Fig. 5b. The deformation of TENG could be regulated by a commercial electromagnet, and the mechanical deformation simulation is presented in Fig. 5c. During the periodic applying–removing magnetic field, this TENG showed real-time assessment capacity with deformation energy harvesting performance. Besides, the deformation of the TENG and the numerical calculations of the electric potential distribution at the pore interface are also proposed to explain the magneto-dependent triboelectric performance (Fig. 5d and e). Fig. 5f shows the sensing signals under various magnetic fields. The TENG device exhibited a distinguished response with a cyclic peak voltage of 77 mV under 75 mT magnetic field, indicating an effective harvesting and sensing performance. Undoubtedly, the peak voltage rose as the magnetic field increased and eventually reached 495 mV in response to 540 mT. The typical voltage response under 410 mT presented good reliability (Fig. 5g). Fig. 5h summarizes the sponge deformation and matching triboelectric signal of the TENG *versus* external magnetic field, which exhibited varied monitoring sensitivity ranging with the magnetic flux density (Fig. S7†). The sponge presented an adjustable configuration as the magnetic field varied, and the deformation rate could be up to 30% under 540 mT. The output voltages exhibited monotonic dependence on magneto-induced deformations, which could be used for precise assessment of external magnetic fields. In addition, the voltage signals exhibited no obvious attenuation after 300 s,

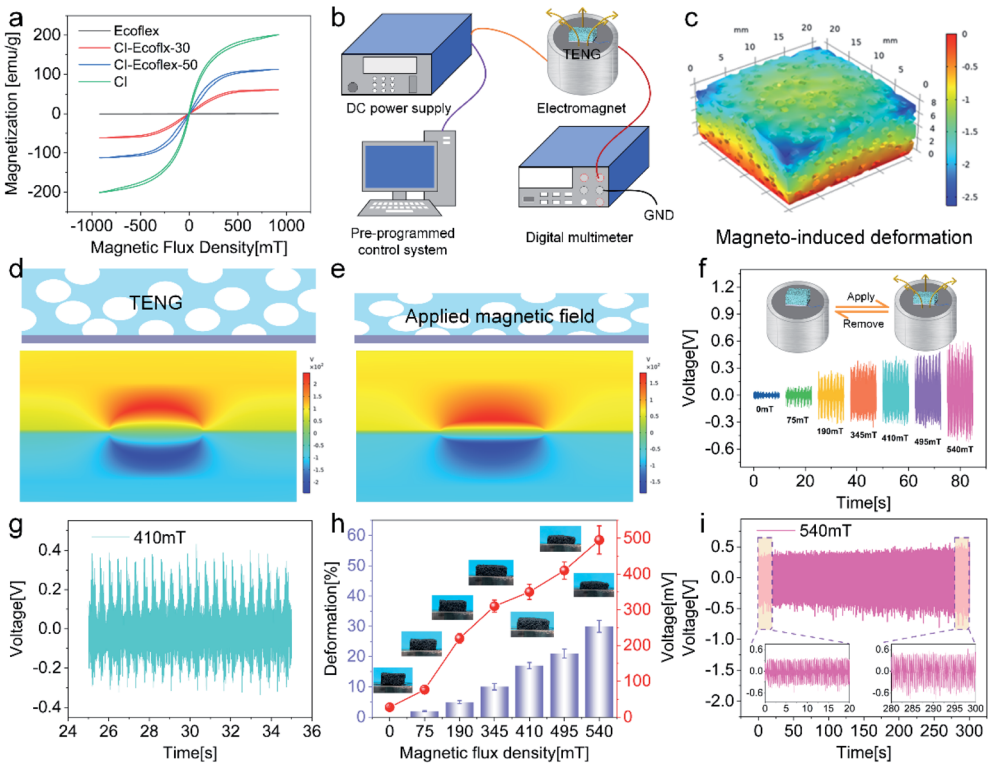

Fig. 5 Magnetic field sensing performance of the TENG device. (a) Magnetic hysteresis loops of various composites. (b) Schematic diagram of the measurement system. (c) Finite-element simulation of the magneto-induced deformation for CI–Ecoflex sponge. (d and e) Mechanical deformation of the TENG under magnetic field and the corresponding numerical calculations of electric potential distribution between contacting interfaces. (f) Magnetic field-dependent triboelectric performance. (g) Typical outputting signals under 410 mT. (h) Magneto-induced sponge deformations and the corresponding voltage signals. (i) Voltage stability of the TENG during cyclic applying–removing 540 mT magnetic field process.

confirming the good cyclic stability (Fig. 5i). To conclude, the as-designed TENG device provided an illuminating strategy for magnetic field monitoring without external power suppliers.

2.4. Smart oil–water separating characteristics of the sponge-based TENG

In recent years, oil leakages and industrial organic solvent emissions led to severe impacts on environmental ecology and economy, so it was of great significance to develop high-efficiency absorbent materials. Due to the low density, high specific surface area and oil storage capacity, various three-dimensional porous structured absorbent materials showed considerable potential for oil–water separation. In particular, porous silicone rubber-based composites turned out to be promising candidates for hydrophobicity, mechanical and chemical stability. In this work, the absorbent capability, smart driving and sensing performance based on the sponge structure of TENG were systematically studied. First, the surface wetting behaviors were explored. When water and oil droplets were dropped on the surface of the sponge, the oil droplet could completely penetrate within 40 s, while water droplet was repelled, revealing its hydrophobicity and lipophilicity (Fig. 6a and b). To fully assess the absorption capacity of the sponge, various oils and organic solvents, consisting of sesame oil, mineral oil, soybean oil, silicone oil, acetone and carbon tetrachloride, were applied in this work. Fig. 6c displays the absorbency values of different oils and organic solvents, and the variation might be related to the viscosity and density of the liquid.[29] Recyclability of absorption behaviors was a crucial indicator for large-scale applications, so a repeated soybean oil adsorption experiment was conducted (Fig. 6d). The sponge was immersed into soybean oil for 30 min and quickly weighed, followed by washing and drying for 3 times. During the cyclic absorbing–releasing process, the sponge showed a stable mass variation, confirming the favorable sustainability. Based on the water repellency and oil affinity, the sponge was endowed with excellent selective adsorption property for removing oil from water. When the sponge approached the carbon tetrachloride droplets under water, it could completely absorb the droplets (Fig. 6e–h). Subsequently, the water became clear, showing excellent performance for recovering heavy oils. More importantly, it exhibited smart magnetic controllable properties. For

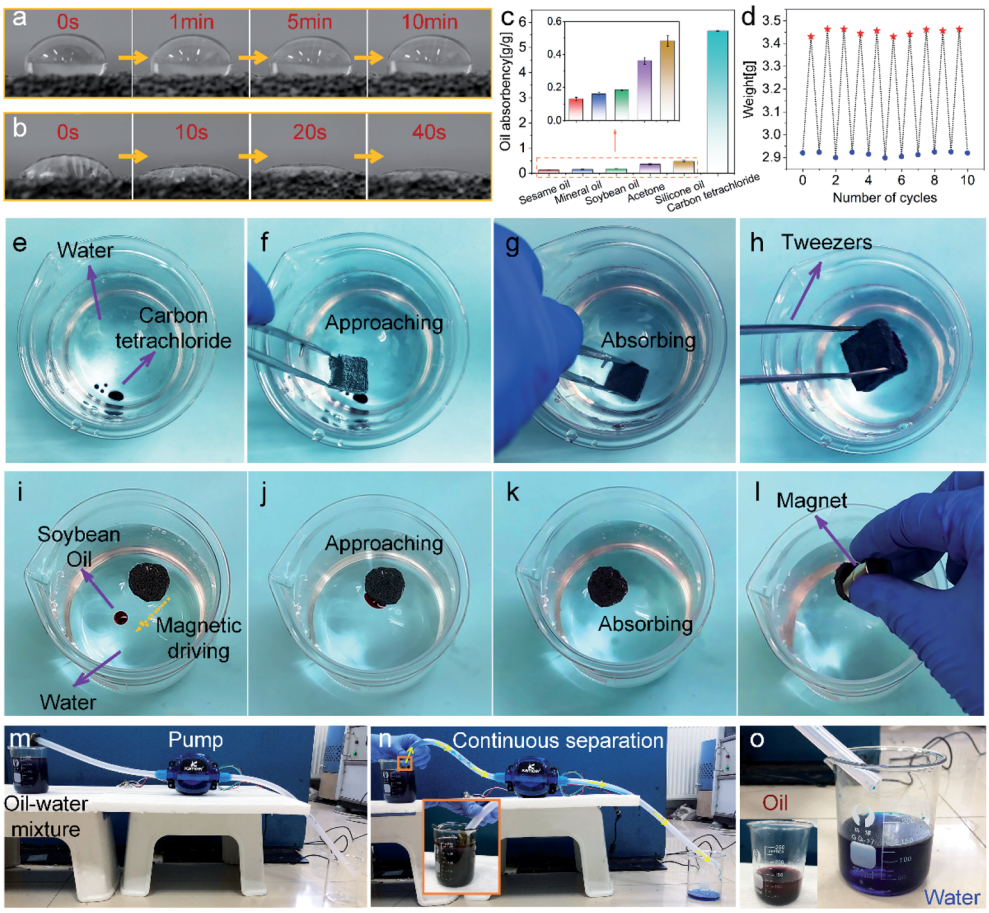

Fig. 6 Oil/water wettability and separation properties of the sponge matrix. Photographs of time evolution for (a) water and (b) mineral oil droplets on the sponge surface. (c) Absorption capacity for various oils and organic liquids. (d) Absorption recyclability for soybean oil. (e–h) Mechanical recovery of carbon tetrachloride under water. (i–l) Magnetically driven removal of soybean oil on the surface of water. (m) The apparatus, (n) process and (o) result of the pump-assisted continuous oil–water separation, in which the soybean oil was colored with oil pigment red and water was labelled with methylene blue for clear observation.

the soybean oil droplet, the sponge on the water surface could be magnetically driven to the target zone, and the droplet could be absorbed (Fig. 6i–l). Then, the sponge was removed from water by a magnet, which offered smart controlling performance of oil–water separation. For practical applications, the oil spills were accumulated before they were disposed, and thus it was necessary to evaluate the continuous separating performance of the absorbent materials. As displayed in Fig. 6m, a continuous oil–water separation apparatus assisted by a peristaltic pump was established, and the polymer sponge acted as a filter functional layer. Once the pump was turned on, the sponge was soaked with oil and the water continuously passed through the pores (Fig. 6n). Eventually, water and oil could be successfully separated and collected using a sponge of $1 \times 1 \times 0.5$ cm^3 dimension (Fig. 6o), implying the desirable oil–water separation capacity.

In addition to the magneto-driven property, the intrinsic triboelectric effect of TENG endowed it with the potential to be used as a smart absorbent material with sensing performance. After infiltration with mineral oil, the sensing properties of the TENG under various applied forces were explored by an electroforce dynamic system (Fig. 7a). To mimic the squeezing–loosening process under practical working conditions, the rectangular wave excitation was applied, with nitrile rubber films as the contact layer. With forces ranging from 2 to 42 N, the responsive voltages exhibited a notable increment from 0.5 to 2.9 V, which could be utilized for precise assessment of external forces (Fig. 7b). As shown in Fig. 7c, the signal was generated at the moment of applying and releasing forces, indicating a favorable monitoring sensitivity. The other oil/organic solvents and the corresponding signal comparison are also displayed (Fig. 7d). In this regard, the TENG served well as a smart absorbent material to perceive and distinguish various absorbed substances during the pressing–releasing process. Besides, a cyclic rectangular wave excitation of 12.0 N was loaded on the TENG soaked with mineral oil, and the peak values demonstrated a small fluctuation during repeated loading–unloading processes for 10 000 s, revealing the potential for stable monitoring (Fig. 7e). To demonstrate the practicability, a TENG-based mineral oil recovery experiment was performed (Fig. 7f). First, the TENG was pre-pressed to remove the air, corresponding to a positive voltage of 0.5 V, and an opposite signal was generated while releasing it. Then an enhanced positive voltage (0.8 V) was obtained once squeezing the oil-filled TENG for recovery, and eventually a negative signal indicated that the TENG was loosened. The reliable sensing property as well as the magneto-actuating characteristic would undoubtedly show the advantage of distinguishing pollutant targets and smart controlling in oil–water separation in complicated surroundings. Moreover, a reasonable mechanism of the effect of oils on the triboelectric performance was proposed (Fig. 7g). Traditionally, a liquid layer on the surface of the silicone rubber composite would contribute to the charge dissipation and weaken the triboelectric performance.[30,31]

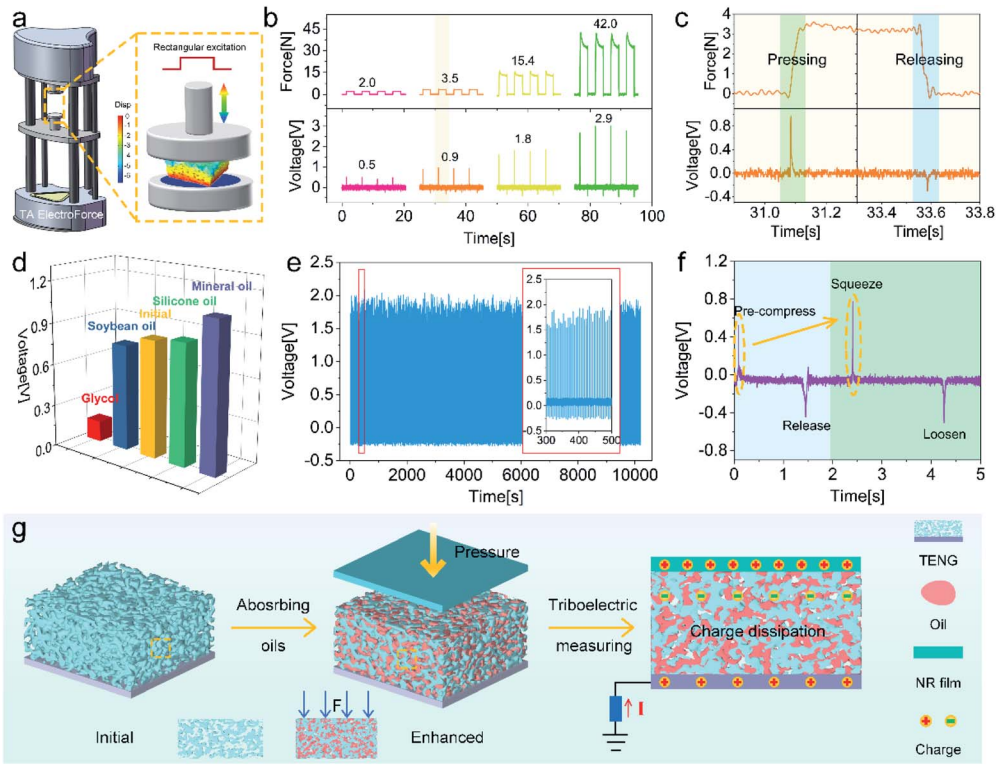

Fig. 7 Intelligent sensing property during oil–water separation. (a) Sensing performance measurement platform. (b) Cyclic variations of the applied force and the corresponding output voltage of the TENG infiltrated with mineral oil. (c) Typical force and voltage changes in one cycle. (d) Comparison of output signals for the TENG infiltrated with various oils. (e) Stability of the mineral oil-soaked TENG under the 12 N compression force. (f) Sensing signal in the process of absorbing mineral oil. (g) Schematic diagram of the effect of oils on the triboelectric performance.

However, the mechanical property of the sponge infiltrated with oils could be enhanced, and the promoting friction effect was beneficial to charge transfer and accumulation. Owing to their antagonism effect, the TENG was endowed with specific perception capacity to different oils.

2.5. TENG-based bi-mode sensor array and wireless sensing system

Based on the unique sponge design, a flexible 3 × 3 sensor array was fabricated with 9 units of 2 × 2 × 1 cm^3 (Fig. 8a-I) to evaluate the external applied force and magnetic field. It was capable of perceiving different compression forces and displaying their distributions *via* corresponding output voltages. As shown in Fig. 8b, when the four units in the upper right region were compressed (Fig. 8a-II), approximate voltage signals of 0.62, 0.64, 0.58 and 0.63 V were generated, while the others exhibited negligible weak voltages, indicating a favorable sensitivity. Similarly, the voltage response varied (Fig. 8c) as the external force stimuli changed (Fig. 8a-III). Fig. 8j gave representative signals of three different units. Furthermore, the calculated potential distributions under different compression conditions by finite element simulation were favourably in agreement with the experiment data, revealing the sensing reliability (Fig. 8d–g). Besides, a magnetic field evaluation system was constructed, in which the magnetic field excitation was applied by a permanent magnet (Fig. 8h). The real-time magnetic field recognition mapping is presented in Fig. 8i. The highest voltage generated from the center unit was 0.85 V, manifesting that it was subjected to a maximum magnetic field. In summary, owing to the sensitive mechanical–magnetic bi-mode monitoring properties and self-powered capacity, the sensor array showed potential applications in smart detection, interaction and control areas.

In consideration of the huge advantage of wireless monitoring networks in practical life, a TENG-enabled wireless passive sensing system was developed. This system consisted of a TENG, microcontroller, a bluetooth module and a cellphone (Fig. 8k and l). To verify the feasibility of the wireless system, the TENG was gently patted (Movie S3†). Undoubtedly, the force and rate of the excitations could be displayed in the cellphone

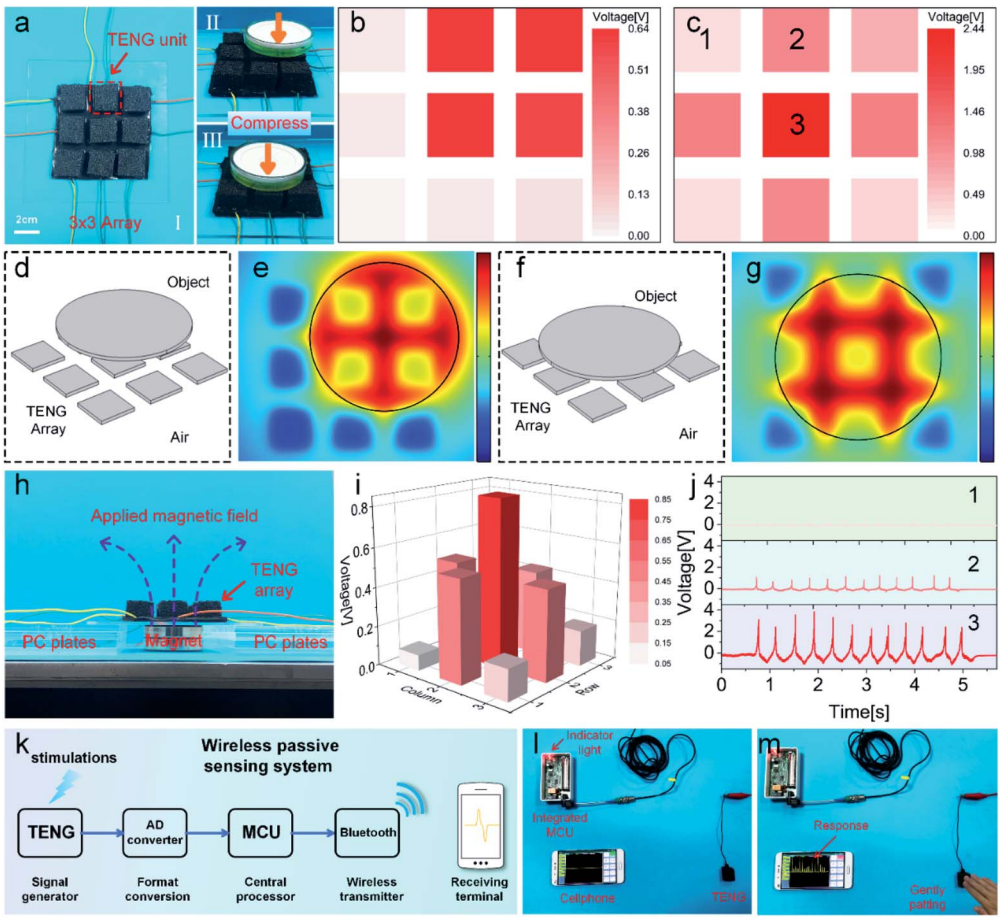

Fig. 8 Demonstrations of the TENG-based mechanical–magnetic dual-mode sensor array and integrated wireless passive sensing system. (a) Photographs of the 3 × 3 sensor array under compression at different regions. (b and c) Recognition capacity for varied pressure distributions. (d–g) Geometric models for numerical calculation and the corresponding simulation results of array electric potential distribution. (h) Assessment system for magnetic field and (i) the corresponding voltage variation distribution. (j) Representative signals of three sensing units under compression. (k) A circuit design schematic diagram of the wireless passive sensing system based on the TENG. (l) Initial and (m) working modes of this system triggered by gentle pats.

(Fig. 8m). Based on the advantages of integration and modularization, the as-designed flexible TENG in this work would greatly promote the development of detection, visualization and early warning systems especially in harsh environments.

3. Conclusion

In summary, a novel multi-functional TENG with mechanical energy harvesting, self-powered magnetic sensing and smart oil–water separating characteristics was developed in this work. It showed favorable triboelectric performance with an optimal instantaneous power density of 71.0 mW m^{-2}, and the effective energy harvesting property enabled it to power small electronics and monitor various human motions. Due to the magneto-actuated deformation performance, it also sensed external magnetic fields. Interestingly, derived from the hydrophobicity and lipophilicity of the sponge matrix, it served well as a smart absorbent material with driving and sensing performance. In addition, this TENG array with mechano-magnetic dual-mode sensing properties could precisely reveal external stimuli distributions, and the integrated wireless system promoted its application under harsh conditions. This work was of guiding significance for the development of sustainable energy sources, self-powered multi-mode sensors and intelligent oil-leakage treatment systems.

Author contributions

Shuai Liu: conceptualization, investigation, methodology, visualization, writing – original draft. Fang Yuan: investigation, formal analysis. Min Sang: investigation, data curation. Jianyu Zhou: formal analysis. Junshuo Zhang: visualization. Sheng Wang: methodology, validation, writing – review & editing. Jinsong Li: Software. Shouhu Xuan: visualization, supervision. Xinglong Gong: resources, supervision, project administration, funding acquisition.

Conflicts of interest

There are no conflicts to declare.

Acknowledgements

Financial supports from the National Natural Science Foundation of China (Grant No. 11802303, 11772320, 11822209, 11972032), the Strategic Priority Research Program of the Chinese Academy of Sciences (Grant No. XDB22040502), and the Joint Fund of USTC-National Synchrotron Radiation Laboratory (KY2090000055) were gratefully acknowledged. This work was partially carried out at the USTC Center for Micro and Nanoscale Research and Fabrication.

References

1 J. N. Deng, X. Kuang, R. Y. Liu, W. B. Ding, A. C. Wang, Y. C. Lai, K. Dong, Z. Wen, Y. X. Wang, L. L. Wang, H. J. Qi, T. Zhang and Z. L. Wang, *Adv. Mater.*, 2018, **30**, 10.
2 A. Shrestha, M. Batmunkh, C. J. Shearer, Y. T Yin, G. G. Andersson, J. G. Shapter, S. Z. Qiao and S. Dai, *Adv. Energy Mater.*, 2017, **7**, 1602276–1602283.
3 J. H. Zhang, Y. Li, J. H. Du, X. H. Hao and H. T. Huang, *J. Mater. Chem. A*, 2019, **7**, 11724–11733.
4 C. He, C. B. Han, G. Q. Gu, T. Jiang, B. D. Chen, Z. L. Gao and Z. L. Wang, *Adv. Energy Mater.*, 2017, **7**, 6.
5 S. Kim, M. K. Gupta, K. Y. Lee, A. Sohn, T. Y. Kim, K. S. Shin, D. Kim, S. K. Kim, K. H. Lee, H. J. Shin, D. W. Kim and S. W. Kim, *Adv. Mater.*, 2014, **26**, 3918–3925.
6 H. J. Guo, T. Li, X. T. Cao, J. Xiong, Y. Jie, M. Willander, X. Cao, N. Wang and Z. L. Wang, *ACS Nano*, 2017, **11**, 856–864.
7 Y. Zou, V. Raveendran and J. Chen, *Nano Energy*, 2020, **77**, 105303.
8 S. B. Jeon, S. Kim, S. J. Park, M. L. Seol, D. Kim, Y. K. Chang and Y. K. Choi, *Nano Energy*, 2016, **28**, 288–295.
9 Z. L. Wang, *Nature*, 2017, **542**, 159–160.
10 Z. L. Wang, *ACS Nano*, 2013, **7**, 9533–9557.
11 X. Cao, Y. Jie, N. Wang and Z. L. Wang, *Adv. Energy Mater.*, 2016, **6**, 21.
12 Y. Liu, Y. Zheng, Z. Wu, L. Zhang, W. Sun, T. Li, D. Wang and F. Zhou, *Nano Energy*, 2021, **79**, 105422.
13 Z. Y. Wu, B. B. Zhang, H. Y. Zou, Z. M. Lin, G. L. Liu and Z. L. Wang, *Adv. Energy Mater.*, 2019, **9**, 7.
14 S. Wang, L. Ding, Y. Wang and X. L. Gong, *Nano Energy*, 2019, **59**, 434–442.
15 Z. M. Lin, B. B. Zhang, H. Y. Guo, Z. Y. Wu, H. Y. Zou, J. Yang and Z. L. Wang, *Nano Energy*, 2019, **64**, 7.
16 J. Wang, H. L. Zhang, Y. H. Xie, Z. C. Yan, Y. Yuan, L. Huang, X. J. Cui, M. Gao, Y. J. Su, W. Q. Yang and Y. Lin, *Nano Energy*, 2017, **33**, 418–426.
17 S. Qi, H. Guo, J. Chen, J. Fu, C. Hu, M. Yu and Z. L. Wang, *Nanoscale*, 2018, **10**, 4745–4752.
18 Z. Zhang, L. Sang, J. Huang, W. Chen, L. Wang, Y. Takahashi, S. Mitani, Y. Koide, S. Koizumi and M. Liao, *Carbon*, 2020, **170**, 294–301.
19 A. Shademani, H. B. Zhang, J. K. Jackson and M. Chiao, *Adv. Funct. Mater.*, 2017, **27**, 9.
20 J. R. Shi, H. B. Zhang, J. Jackson, A. Shademani and M. Chiao, *J. Mater. Chem. B*, 2016, **4**, 7415–7422.
21 Y. Wang, L. N. Zhang and A. Lu, *J. Mater. Chem. A*, 2020, **8**, 13935–13941.
22 H. Guo, J. Chen, L. Wang, A. C. Wang, Y. Li, C. An, J.-H. He, C. Hu, V. K. S. Hsiao and Z. L. Wang, *Nat. Sustainability*, 2021, **4**, 147–153.
23 X. Zhao, L. Li, B. Li, J. Zhang and A. Wang, *J. Mater. Chem. A*, 2014, **2**, 18281–18287.
24 J. Ge, L.-A. Shi, Y.-C. Wang, H.-Y. Zhao, H.-B. Yao, Y.-B. Zhu, Y. Zhang, H.-W. Zhu, H.-A. Wu and S.-H. Yu, *Nat. Nanotechnol.*, 2017, **12**, 434–440.
25 T. L. Yu, F. Halouane, D. Mathias, A. Barras, Z. W. Wang, A. Q. Lv, S. X. Lu, W. G. Xu, D. Meziane, N. Tiercelin, S. Szunerits and R. Boukherroub, *Chem. Eng. J.*, 2020, **384**, 9.
26 C. F. Wang, H. C. Huang and L. T. Chen, *Sci. Rep.*, 2015, **5**, 8.

27 L. L. Zhao, L. Q. Liu, X. Y. Yang, H. X. Hong, Q. M. Yang, J. W. Wang and Q. W. Tang, *J. Mater. Chem. A*, 2020, **8**, 7880–7888.
28 S. Wang, L. Ding, X. W. Fan, W. Q. Jiang and X. L. Gong, *Nano Energy*, 2018, **53**, 863–870.
29 X. Y. Wang, Y. Lu, C. J. Carmalt, I. P. Parkin and X. Zhang, *Langmuir*, 2018, **34**, 13305–13311.
30 K. Y. Lee, J. Chun, J. H. Lee, K. N. Kim, N. R. Kang, J. Y. Kim, M. H. Kim, K. S. Shin, M. K. Gupta and J. M. Baik, *Adv. Mater.*, 2014, **26**, 5037–5042.
31 J. A. Wiles, M. Fialkowski, M. R. Radowski, G. M. Whitesides and B. A. Grzybowski, *J. Phys. Chem. B*, 2004, **108**, 20296–20302.